# Characterizing Multiphase Organic/Inorganic/Aqueous Aerosol Droplets

**Jariya Buajarern, Laura Mitchem, and Jonathan P. Reid***

*School of Chemistry, University of Bristol, Bristol, BS8 1TS, U.K.*

*Received: June 6, 2007; In Final Form: July 16, 2007*

The partitioning of an immiscible and volatile organic component between the gas and aqueous condensed phases of an aerosol is investigated using optical tweezers. Specifically, the phase segregation of immiscible decane and aqueous components within a single liquid aerosol droplet is characterized by brightfield microscopy and by spontaneous and stimulated Raman scattering. The internally mixed phases are observed to adopt equilibrium geometries that are consistent with predictions based on surface energies and interfacial tensions and the volume fractions of the two immiscible phases. In the limit of low organic volume fraction, the stimulated Raman scattering signature is consistent with the formation of a thin film or lens of the organic component on the surface of an aqueous droplet. By comparing the nonlinear spectroscopic signature with Mie scattering predictions for a core−shell structure, the thickness of the organic layer can be estimated with nanometer accuracy. Time-dependent measurements allow the evolving partitioning of the volatile organic component between the condensed and vapor phases to be investigated.

## I. Introduction

Tropospheric aerosol is a complex mixture of inorganic and organic components.[1−3] Depending on location, the organic component typically represents 20−50% of the total aerosol mass and covers a wide range of molecular polarities and weights.[4] Currently, the mixing state of the organic component in tropospheric aerosols is poorly understood.[5−10] While some organic components are soluble and can be expected to be dispersed throughout an aqueous phase, other organic components can be insoluble or immiscible. Although the organic component may be present as an internal mixture, with both components existing within a single particle, phase segregation can lead to the existence of primarily organic and aqueous domains. Indeed, it has been recommended that the presence of liquid or amorphous organic phases at low relative humidity must be considered to interpret the properties of tropospheric aerosol.[8] Phase separation of organic and aqueous components can affect aerosol hygroscopicity and toxicity and can influence the partitioning of trace organic components between the vapor and condensed phases.

The presence of an inorganic salt affects the activities of aqueous and organic components, influencing not only their partitioning between the vapor and condensed phases but also altering the miscibility of the two condensed phase components.[8] The most stable thermodynamic state may be for nonpolar organic molecules to accumulate in a phase-separated state rather than be dispersed throughout an aqueous phase. Further, it has been demonstrated that the partitioning of an organic component between two immiscible phases can be dependent on the concentration of an inorganic salt.[11,12] An examination of the phase partitioning of butanoic acid in an aqueous sodium chloride solution established that an increase in the aqueous concentration of sodium chloride leads to a decrease in the partitioning of the organic component in the aqueous phase and an increase in the mass fraction of the phase-separated organic component.[11] Indeed, the complete separation of the aqueous and organic phases could lead to an aerosol for which the water uptake is similar to that of a pure sodium chloride solution.

Not only may the existence of discrete domains of aqueous and organic phases have a profound impact on the thermodynamic properties of organic/inorganic/aqueous aerosol but also the optical properties and kinetics of mass transfer and heterogeneous reactions can be influenced. The single scattering albedo is not simply dependent on particle size and, thus, hygroscopicity but on mixing state and the presence of phase inclusions.[13] Further, an organic component can partition preferentially to the surface of an aerosol droplet leading to a surface excess or the formation of an insoluble organic surface film.[14] Such heterogeneity in composition can influence the rate of mass transfer between the gas and condensed phases and can alter the heterogeneous chemical reactivity. Further, many experimental studies have provided evidence that sea-salt aerosol particles can contain a surface organic layer.[15,16] Tervahattu et al.[17] suggested that the existence of such an organic surface film can play a role in the partitioning of semivolatile organic compounds in the marine or coastal environment. For example, enhancement of organic absorption has been observed on an organic coated surface.[18]

In this publication we demonstrate that the coupling of aerosol optical tweezers with brightfield microscopy[19] and Raman spectroscopy[20] can be used to investigate the phase behavior and surface partitioning of mixed organic/inorganic/aqueous aerosols. Decane (specifically *n*-decane) is chosen as a benchmark system representative of volatile insoluble organic components. The dependence of the physical distribution of the phase-segregated organic and aqueous components on the volume fractions of each component is investigated. Further, decane is volatile with a vapor pressure of 100 Pa at 16.7 °C. Thus, the partitioning of the organic and aqueous components is anticipated to vary with time as the volume fraction of the decane decreases at constant relative humidity. The mixed phase droplets are formed by the coagulation of initially externally mixed organic and aqueous aerosol.

* To whom correspondence should be addressed. E-mail: j.p.reid@bristol.ac.uk.

10.1021/jp074366a CCC: $37.00 
Published on Web 08/24/2007

The experimental technique is first described in Section II. In Section III, we present predictions of the equilibrium shape of multiphase droplets of varying aqueous and organic volume fractions, before comparing the predictions with typical observations of the shape of composite decane/aqueous sodium chloride droplets. Finally in Section IV, we consider the formation of organic surface films at long times after coagulation following the evaporation of the decane component to a volume fraction considerably lower than at the point of coagulation. By comparing the spectroscopic signatures with Mie scattering calculations performed on core−shell droplets, we demonstrate that the evolution in film thickness can be investigated as the organic component continues to evaporate.

## II. The Experimental Technique

The aerosol tweezing measurements have been performed on two instruments, both of which have been described in detail in previous publications and only a brief summary of the key components will be described here.[21,22] The first instrument is based around a commercial Leica DM IRB microscope and employs an Ar-ion laser operating at 514.5 nm. The second instrument is based around a custom built design employing a Nd:YVO4 laser (Coherent VERDI V5) operating at 532 nm. At wavelengths between 500 and 550 nm, the complex refractive index of water is $<10^{-8}$, minimizing laser induced heating of the droplet through absorption. The optical trap is formed in each system by focusing the light through either a 60× or 100× oil immersion objective. Images of the trapped droplets are recorded by conventional brightfield microscopy. Backscattered Raman light is dispersed with a 0.5 m spectrograph (Spectra Pro 2500i Acton Research Corporation), equipped with a diffraction grating (1200 g/mm), and analyzed with a CCD camera (Princeton Instruments). The Raman spectra are acquired with a spectral dispersion of 0.05 nm/pixel with a 1 s time integration, unless otherwise stated.

Aqueous aerosol is generated from an aqueous sodium chloride solution of concentration 0.34 M using an ultrasonic nebulizer (Omron NE-U07). The sodium chloride reduces the vapor pressure of the droplet, allowing it to be retained indefinitely in the optical trap under subsaturated conditions.[19] The organic aerosol is also generated with an ultrasonic nebulizer using pure decane. In the majority of the measurements presented here, an aqueous droplet is initially loaded into an optical trap and is then bombarded with decane aerosol. Prolonged dosing increases the volume of decane mixed with the aqueous droplet through discrete coagulation events. In studies in which the organic volume fraction dominates the aqueous component, the order is reversed and a decane droplet is initially loaded into the trap, followed by subsequent dosing with aqueous aerosol.

## III. Examining the Equilibrium Configuration of Organic/Inorganic/Aqueous Multiphase Droplets

Torza and Mason[23] developed a model to describe the equilibrium configuration observed when two immiscible liquid droplets (phases 1 and 3) are brought into contact surrounded by a further immiscible phase (phase 2). The resulting configuration can be predicted from the interfacial tensions and spreading coefficients of the various components and the volumes of the individual droplets prior to contact. The key details and definitions pertinent to aerosol measurements are only briefly reviewed here and the reader is referred to reference 23. Phase 1 corresponds to the aqueous phase, phase 3 to the decane phase, and phase 2 to the gas phase.

An interface between phases 1 and 3 forms when immiscible liquid aerosol droplets of radii $a_1$ and $a_3$ are brought into contact, as illustrated in Figure 1. A cross-section through the composite droplet is shown, along with the angles that define the equilibrium shape of the composite droplet formed and the radii of curvature $r_{ij}$ of the two immiscible spherical segments. The final equilibrium state is determined by the three interfacial tensions denoted by $\sigma_{ij}$. The state of the equilibrium configuration is assumed to be independent of fluid motion, and gravitational and interparticle forces, although in practice these factors may be important in promoting its attainment. The equilibrium state of the three phases is defined by the geometrical configuration which has a minimum surface energy. Equilibrium configurations can be classified into three types: complete engulfing, partial engulfing, and non-engulfing, in which the two liquid droplets remain as individual single droplets.

The shape factor, $R$, is defined as the ratio of the radius of curvature of phase 1, $r_{12}$, over the radius of curvature of phase 3, $r_{23}$.

$$R = r_{12}/r_{23} \tag{1}$$

The interface is described by a radius of curvature of $r_{13}$. The shape factor of the composite droplet can be related to the ratio of the initial droplet radii, $R_0$, prior to contact,

$$R_0 = a_1/a_3 \tag{2}$$

and the angles defined in Figure 1.

$$\frac{R_0^{\,3}}{R^3} = \frac{2 + \cos\phi_{12}(3 - \cos^2\phi_{12}) + (\Gamma_1 - R\Gamma_3)^{-3}[2 - \cos\phi_{13}(3 - \cos^2\phi_{13})]}{2 + \cos\phi_{23}(3 - \cos^2\phi_{23}) - R^3(\Gamma_1 - R\Gamma_3)^{-3}[2 - \cos\phi_{13}(3 - \cos^2\phi_{13})]} \tag{3}$$

$\Gamma_1$ and $\Gamma_3$ are defined as the ratios of the surfacial/interfacial tensions,

$$\Gamma_1 = \frac{\sigma_{12}}{\sigma_{13}},\ \Gamma_3 = \frac{\sigma_{23}}{\sigma_{13}} \tag{4}$$

The surface tensions of decane and an aqueous sodium chloride solution (0.34 M) at 20 °C are 23.8 and 73.4 mN/m, respectively.[24,25] The interfacial tension between decane and the 0.34 M sodium chloride aqueous phase can be estimated to be 51.3 mN/m.[26] For a selected shape factor $R$, the angles $\phi_{ij}$ describing the composite shape of the droplet can be calculated from eqs 5−7.

$$\cos\phi_{12} = \frac{2\Gamma_1\Gamma_3 R - (\Gamma_1^{\,2} + \Gamma_3^{\,2} - 1)}{2\{\Gamma_1\Gamma_3[\Gamma_1\Gamma_3(R^2 + 1) - R(\Gamma_1^{\,2} + \Gamma_3^{\,2} - 1)]\}^{1/2}} \tag{5}$$

$$\cos\phi_{13} = \frac{R\Gamma_3(\Gamma_1^{\,2} - \Gamma_3^{\,2} + 1) - \Gamma_1(\Gamma_1^{\,2} - \Gamma_3^{\,2} - 1)}{2\{\Gamma_1\Gamma_3[\Gamma_1\Gamma_3(R^2 + 1) - R(\Gamma_1^{\,2} + \Gamma_3^{\,2} - 1)]\}^{1/2}} \tag{6}$$

$$\cos\phi_{23} = \frac{2\Gamma_1\Gamma_3 - R(\Gamma_1^{\,2} + \Gamma_3^{\,2} - 1)}{2\{\Gamma_1\Gamma_3[\Gamma_1\Gamma_3(R^2 + 1) - R(\Gamma_1^{\,2} + \Gamma_3^{\,2} - 1)]\}^{1/2}} \tag{7}$$

Knowledge of the angles and radii of the composite droplet for a selected $R$ then allows calculation of the ratio of the initial droplet radii, $R_0$, prior to intimate contact.

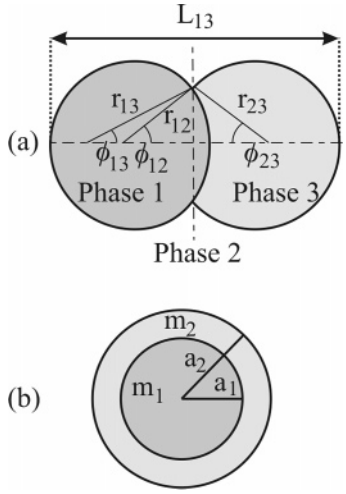


**Figure 1.** (a) Configuration of two immiscible droplets defining the geometrical parameters that define the shape of the biphase aerosol droplet. The radii of curvature, $r_{12}$ and $r_{23}$, define the circles of curvature describing the gas-liquid surfaces of phases 1 and 3, respectively. The radius of curvature $r_{13}$ defines the circle of curvature describing the shape of the interface between phases 1 and 3. It should be noted that the centers of these circles do not necessarily coincide, as is apparent in the figure. (b) Schematic of a core-shell layered droplet showing the inner and outer radii.

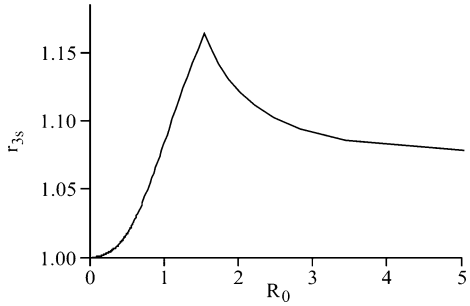


**Figure 2.** The theoretically predicted relationship between $r_{3s}$ and $R_0$ for decane/aqueous sodium chloride droplets.

Two remaining quantities must be determined to define the shape of the composite droplet. The axis ratio, $r_{3s}$, indicates the relative configuration of the two immiscible liquid phases and provides an inverse measure of the degree of engulfing. The axis ratio can be determined from eqs 8 and 9,

$$r_{3s} = L_{13}/2r^* \tag{8}$$

where

$$L_{13} = r_{12}(1 + \cos\phi_{12}) + r_{23}(1 + \cos\phi_{23}) \tag{9}$$

and $r^*$ is the greater of $r_{12}$ and $r_{23}$. Thus, when the axis ratio is unity, one component is completely engulfed within the second, with the second having a radius $r^*$.

Figure 2 illustrates the theoretical relation between $r_{3s}$ and $R_0$ for a composite decane/aqueous sodium chloride droplet, defining the relative position of the decane phase with reference to the aqueous phase. As the value of $R_0$ increases above 1, the radius of the aqueous droplet becomes larger than the radius of the decane droplet prior to coagulation. At $R_0 \approx 1.5$, $r_{3s}$ reaches a maximum value, at which point the degree of engulfing is at a minimum. The quantities $r_{ij}$ and $\phi_{ij}$, which describe the equilibrium configuration of two immiscible droplets, are summarized in Table 1 for a composite droplet for which $r_{12}$, the radius of the aqueous phase in the composite droplet, is equal to 3 $\mu$m. It can be seen from these data that the equilibrium configuration of a composite decane/aqueous sodium chloride droplet is dependent on the relative sizes of the two droplets prior to coagulation.

**TABLE 1: Quantities Describing the Equilibrium Shape of Two Immiscible Spherical Segments Assuming $r_{12} = 3.00$ $\mu$m[a]**

| $R_o$ | $r_{12}$ $\mu$m | $r_{23}$ $\mu$m | $r_{13}$ $\mu$m | $\phi_{12}$ deg | $\phi_{23}$ deg | $\phi_{13}$ deg |
|---|---|---|---|---|---|---|
| 0.44 | 3.00 | 6.00 | 2.58 | 126.8 | 33.9 | 117.1 |
| 0.90 | 3.00 | 3.75 | 2.93 | 99.6 | 61.3 | 90.8 |
| 1.15 | 3.00 | 3.33 | 3.06 | 89.8 | 71.2 | 81.3 |
| 1.51 | 3.00 | 3.00 | 3.21 | 80.5 | 80.5 | 72.3 |
| 2.09 | 3.00 | 2.73 | 3.37 | 72.1 | 88.9 | 64.1 |
| 3.73 | 3.00 | 2.50 | 3.56 | 64.6 | 96.3 | 57.1 |

[a] Phase 1, 2, and 3 refer to the aqueous, air, and decane phases, respectively.

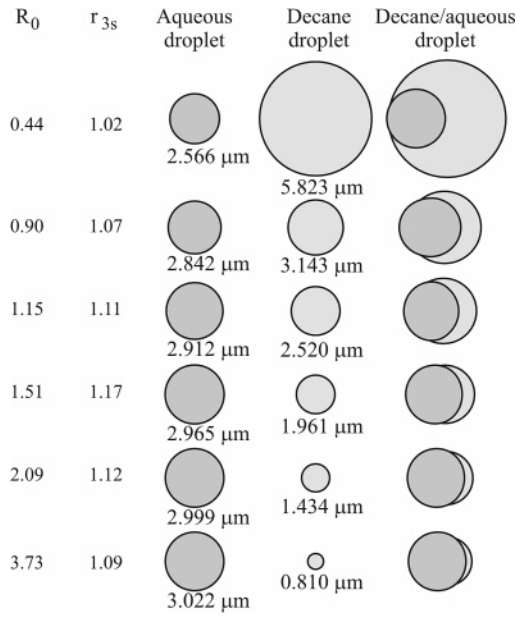


**Figure 3.** Calculated configurations for composite decane/aqueous sodium chloride droplets for various aqueous/decane mixing volume ratios.

The loci of the phase boundaries defined by eqs 1−9 are calculated and illustrated in Figure 3 for composite decane/aqueous sodium chloride droplets starting from aqueous and decane droplets of varying radii. When the decane droplet radius is much larger than the aqueous droplet, $R_0 < 0.44$, complete engulfing of the aqueous droplet by the host decane droplet is observed. At $R_0 \geq 0.44$, a partial engulfing configuration is predicted. For $R_0 \geq 1.5$, the volume fraction of decane is so much smaller than that of water that it can be considered to form a surface lens. At no stage is a decane droplet completely engulfed within an aqueous host droplet.

The equilibrium configurations observed following the coagulation of decane droplets with aqueous sodium chloride droplets of varying relative sizes were investigated experimentally. A representative sample of images from composite droplets is shown in Figure 4. It should be noted that the images provide only a two-dimensional perspective from the bottom view. The images are ordered such that the three groups 4a, 4b−e, and 4f display different configurations. The composite droplets shown in Figure 4b−e were formed by coagulating aqueous aerosol droplets with a large optically trapped decane droplet, ensuring the dominance in volume fraction of the organic phase. In Figure 4a and f an aqueous droplet was first trapped and varying amounts

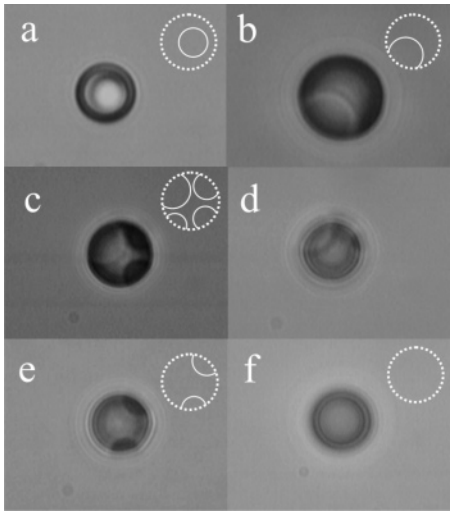


**Figure 4.** Images of composite decane/aqueous sodium chloride droplets observed in various configurations arising from different volume ratios of the organic and aqueous phases. The observed extent of the phase boundaries are highlighted schematically, with a dotted line defining the extent of the decane phase and the solid line the extent of the aqueous phase. It should be noted that the image is a two dimensional projection and the full extent of the inclusion is often not apparent.

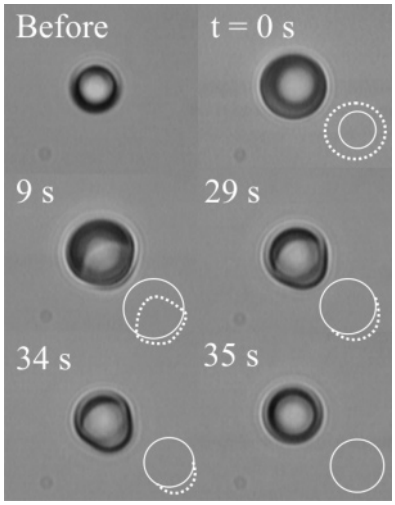


**Figure 5.** The temporal dependence of a decane/sodium chloride aqueous droplet after coagulation. The observed phase boundaries are shown schematically, with a dotted line defining the extent of the decane phase and the solid line the extent of the aqueous phase.

of decane added through coagulation. It is assumed that in each coagulation and at all times the composite droplet exists in an equilibrium state, governed by the treatment presented earlier in this section.

The structures observed are broadly consistent with the predictions, exhibiting a range of partially engulfed structures. A simple schematic of the observed phase boundaries is included in five of the images to highlight the apparent partitioning of the organic and aqueous components from the image. Although an aqueous droplet was observed to undergo complete engulfing by a decane droplet (Figure 4a), complete engulfing of decane by the aqueous phase was not observed, and this is consistent with the predictions. Frequently, multiple small inclusions were observed to form which over time amalgamated to form a single inclusion. For example, the presence of multiple aqueous inclusions is evident in images 4b−e. Figure 4f represents an image of a composite droplet resulting from coagulation of an aqueous droplet with a small decane droplet in which no phase segregation was observed. In future measurements, we intend to obtain an image of the droplet from the side as well as recording an in-plane image to allow a detailed picture of phase segregation to be achieved.[27]

Following coagulation, decane evaporates rapidly from the droplet into the gas-phase, where the partial pressure of decane rapidly decreases below the vapor pressure of decane. By contrast, the vapor pressure of the aqueous component is approximately balanced by the gas-phase partial pressure. This change in droplet composition leads to an equilibrium configuration that changes with time. The translation of the phase boundary can be followed by brightfield microscopy, providing an unambiguous assignment of the two phases seen in the image. This can be confirmed from the accompanying spectroscopic signature that provides a spatially resolved measure of the composition along the central axis of the droplet.[21] The decane component resides centered in the trap in images 4b−e. This may be a consequence of it being the originally trapped and dominant component.

A further example of complete engulfing of an aqueous droplet within a decane host droplet is shown in Figure 5. During decane evaporation, the decane volume becomes smaller than the aqueous phase volume, leading from complete engulfing to a partial engulfing configuration. Before 9 s, the component trapped directly by the optical field switches from the decane to the aqueous component, which becomes the dominant phase during the subsequent rapid evaporation of decane. The decane/aqueous interface is observed to change in shape with decreasing decane volume. At 34 s after coagulation, the decane volume is very small compared to the aqueous volume and the shape clearly resembles the geometries predicted when the water component dominates the decane component. However, 35 s after coagulation, the discrete decane phase is no longer evident. It is interesting to consider at this point if the decane is rapidly lost by evaporation, by phase separation into two droplets, or through the spreading of decane on the surface. In the latter case, a complete decane layer coating the droplet or a thin lens not apparent in the image may form.

## IV. Spectroscopy of Deformed and Layered Droplets

In previous work, we have demonstrated that spontaneous Raman scattering can be used to determine droplet composition with spatial resolution, with the spontaneous scatter arising from the volume of the droplet through which the tweezing laser beam propagates.[21,28] We have also demonstrated that stimulated Raman scattering (SRS) from optically trapped aqueous aerosol allows the droplet size to be determined with nanometer accuracy.[22] Both the spontaneous and stimulated components are observed in a Raman fingerprint, collectively referred to as a cavity enhanced Raman scattering (CERS) fingerprint.[20,29]

CERS fingerprints are shown in Figure 6 at a range of times prior to and post coagulation of an aqueous sodium chloride droplet with an optically trapped decane droplet. Initially, intensity originates from Raman active C−H stretching vibrations of decane.[21] Sharp resonance peaks arising from SRS are observed superimposed on the spontaneous Raman band, appearing only at wavelengths that are commensurate with whispering gallery modes (WGMs). The wavelengths of the WGMs can allow the accurate determination of droplet size.[20,29] WGMs provide a mechanism for optical feedback and lead to SRS surpassing threshold. Following coagulation at a time of 0 s, the substantive phase segregation, such as that shown in Figure 4, inhibits the formation of high quality WGMs,

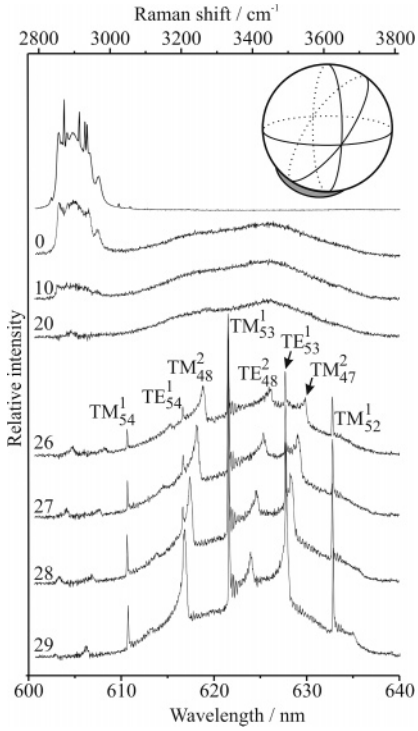


**Figure 6.** The variation in the CERS fingerprint of a decane/aqueous sodium chloride droplet following coagulation. The time is indicated at the left of each spectrum in seconds. The inset schematic illustrates the possible impact of a non-uniform coating on the degeneracy of the azimuthal modes of the same order and number. It is not possible to reconcile the appearance of the SRS fingerprint with the brightfield images; although the spectroscopy suggests considerable deviations in sphericity, the deviations remain smaller that it is possible to resolve in the acquired images.

quenching the SRS signal, and only spontaneous Raman scattering is observed.[21] The decane component is lost by evaporation to the gas-phase leading to a diminishing C−H stretching signature with time. The trapped droplet that was initially decane is predominantly water at times after 20 s.

At a time of 26 s following coagulation, SRS once again surpasses threshold and a complex pattern of WGMs is observed in the spectrum extending over both the O−H and C−H Raman bands of the aqueous and decane components, respectively. An assignment of the WGMs is indicated based on Mie scattering calculations for a core−shell structure described below;[30] the pattern of WGM wavelengths is best fit by assuming a spherical aqueous sodium chloride core coated by a decane shell, as illustrated in Figure 1b. TE and TM refer to transverse electric and transverse magnetic modes, respectively.[20,29] The subscript in the notation refers to the mode number, the number of wavelengths forming the standing wave around the droplet circumference. The superscript refers to the mode order, the number of maxima in the radial dependence of the light intensity within the droplet.[20,29]

While the first-order modes are observed to remain at the same wavelengths over the time period 26 to 29 s in Figure 6, the second-order modes are observed to shift to the blue with time. This could be consistent with an aqueous droplet core (4.3 $\mu$m radius) surrounded by a decane shell ($\sim$1 $\mu$m) that is changing rapidly in thickness with time.[30] Further, the second-order modes are highly asymmetric and are shaded toward blue wavelengths. This suggests that the droplet can only be approximately described by a core−shell structure and is in fact deformed from sphericity.[31]

The CERS fingerprints observed in Figure 6 are broadly consistent with the prediction that a surface lens of decane may form on the surface of an aqueous droplet when the volume fraction of decane is very low. Under these circumstances, the droplet does not retain spherical symmetry and the discrete step in refractive index between the core and shell is not uniform over the whole droplet surface. For a perfect sphere, each WGM has an azimuthal degeneracy of $(2n + 1)$ with each mode having the same path length around the droplet circumference and all modes appearing at the same wavelength. When a droplet is distorted from sphericity, or has an inhomogeneity in refractive index such as that discussed here, the $(2n + 1)$ WGMs no longer retain identical pathlengths and this leads to their appearance at slightly different wavelengths within the spectral fingerprint.[32,33] This results in the splitting or broadening of WGMs, as suggested by the inset to Figure 6.

The influence of such spatially nonuniform films/lenses on the WGM wavelengths of different azimuthal modes has not been considered to our knowledge, and a detailed theoretical treatment is beyond the remit of this publication. However, in the limit of very low decane volume fractions and long times following coagulation, the mode pattern becomes simpler and the degeneracy of different azimuthal modes is restored. In this publication we will limit our quantitative analysis to the discussion of this behavior, which occurs at times exceeding a few minutes after coagulation.

The light circulating in a WGM penetrates to a depth of $\sim a - a/m$ from the interface, where $m$ is the refractive index of a droplet of radius $a$.[34] Inhomogeneities in refractive index within this penetration depth influence the wavelengths at which resonances are observed. In particular, the presence of a thin shell of refractive index $m_2$ on a droplet of total radius $a_2$ surrounding a core of refractive index $m_1$ and radius $a_1$ (Figure 1b) influences the spacing between adjacent TM and TE modes.[35−38] By comparing the experimental WGM wavelengths with Mie scattering calculations for such a core−shell structure, the thickness and refractive index of the shell, and the radius and refractive index of the core, can be determined.

The Mie scattering problem of a sphere consisting of a core and concentric spherical layers of different components was first considered by Aden and Kerker in 1951.[39] More recently, Ray et al.[40] reported the scattering spectra observed for a glycerol sphere ($m_1 = 1.471$) coated with a dioctyl phthalate layer ($m_2 = 1.484$). Even for layer thicknesses of less than 1.5% of the particle size, slight shifts were observed in the resonance wavelengths relative to those for a homogeneous sphere. As the layer thickness increases, differences are observed between the spectra for a layered sphere and a homogeneous sphere of the core component. When the layer is very thick (>20% of the particle radius) the WGMs do not penetrate to the droplet core but circulate only in the surface layer. Thus, the WGMs are unaffected by the presence of the core. In this large layer thickness limit, the fingerprint of WGM wavelengths is almost identical to that observed for an homogeneous droplet of the layer component.

In this publication we consider Mie scattering calculations for a core−shell droplet performed using the coated sphere code developed by Wiscombe.[41] The refractive index of aqueous sodium chloride is assumed to follow the concentration and wavelength dependence described in reference 42 and the refractive index of decane is 1.411.[25] The relative wavelengths of TE and TM modes are compared in Figure 7a for an aqueous sodium chloride droplet core of 3 $\mu$m coated in a decane layer of thickness 10, 50, or 100 nm. With increasing layer thickness,

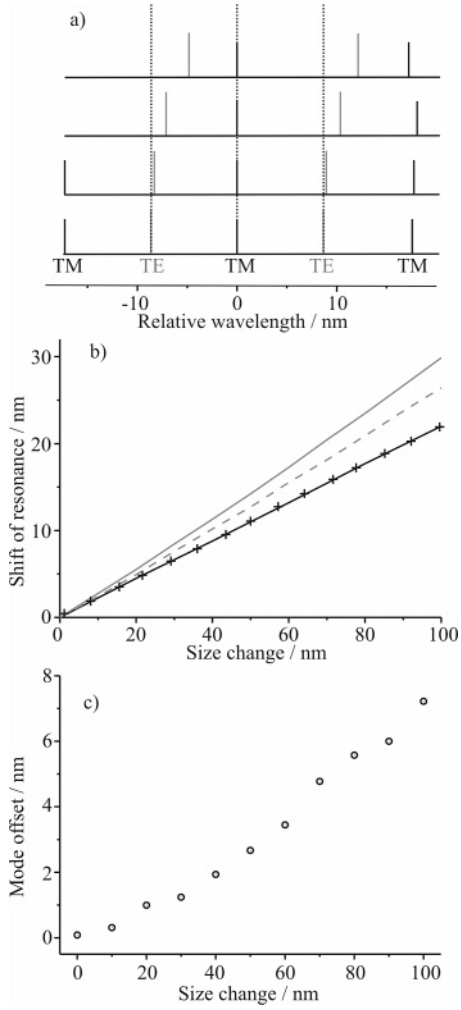


**Figure 7.** (a) An illustration of the different wavelength shifts of TE and TM modes with increasing layer thickness of decane (0, 10, 50, and 100 nm thick layers, from bottom to top) for a 3 $\mu$m core radius aqueous sodium chloride droplet. (b) Calculated spectral shifts of the $TE_{35}$ and $TM_{34}$ resonances from their initial wavelengths for a 3 $\mu$m radius sodium chloride aqueous droplet as a function of size change due to homogeneous growth (black line TE mode, cross symbols TM mode) or the formation of a decane layer (TE solid grey line, TM dashed grey line). (c) Mode offset of the TM mode relative to the TE modes for an aqueous sodium chloride droplet, radius 3 $\mu$m, with increasing decane layer thickness.

an increasing shift in the TE modes relative to those for the uncoated homogeneous aqueous droplet is apparent.

The calculated wavelength shifts of TE and TM modes occurring with increasing droplet size are summarized in Figure 7b. Calculated wavelength shifts are compared for simple homogeneous growth of the aqueous sodium chloride droplet and growth through the deposition of a layer of decane on the surface of an aqueous core. The magnitude of the wavelength shift is dependent on the change in droplet size and the refractive index of the growing component.[30] For the case of homogeneous droplet growth, the TE and TM mode shifts are identical, and a small increase in droplet size leads to an equal red shift of resonance wavelengths. When the size change occurs due to the formation/growth of a layer of decane on the aqueous surface, the TE modes shift by a greater amount that the TM modes, reflecting the trend observed in Figure 7a. As a first approximation, examining the wavelength of a TM mode in relation to two neighboring TE modes provides a method for assessing the existence of decane layers, or organic layers in general, on the surface of an aqueous droplet. Thus, the

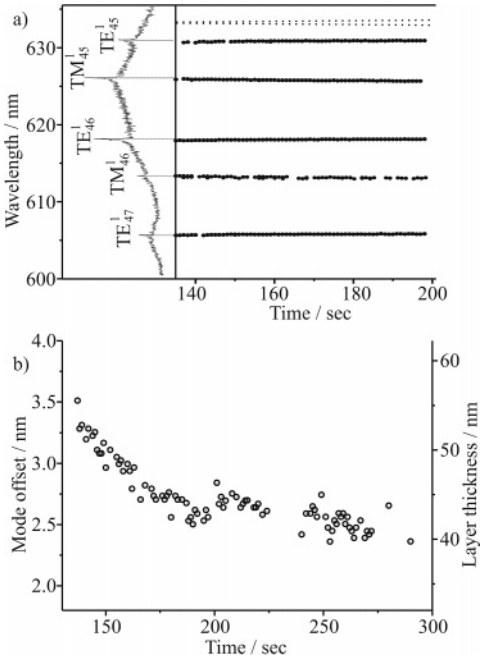


**Figure 8.** (a) The temporal variation in the WGM wavelengths with time following coagulation. The relative shifts of the TE and TM modes are apparent, characteristic of a core-shell droplet with changing shell thickness. The $TE_{46}$ mode red shifts 0.15 nm whilst the $TM_{45}$ blue shifts 0.25 nm, giving rise to a change in mode offset. The gradients of these two shifts are compared by the dotted lines shown at the top of the time dependent data. (b) Variation in the mode offset with time of the $TM_{45}$ ($l = 1$) mode relative to the $TE_{45}$ and $TE_{46}$ ($l = 1$) modes and the change in layer thickness estimated for a decane/aqueous sodium chloride droplet.

difference in wavelength spacing between TM and TE modes to higher and lower wavelength, can be use to interrogate the layer thickness. In the analysis which follows, this difference is referred to as the mode offset. When the mode offset is zero, the TM mode lies halfway between the neighboring TE modes. In Figure 7c we illustrate how the mode offset varies with increase in organic layer thickness on a core aqueous sodium chloride droplet of 3 $\mu$m radius.

The evolving CERS fingerprint from a composite decane/aqueous sodium chloride droplet following coagulation is shown in Figure 8a. Initially, inhomogeneities in refractive index are so severe that the SRS signal is suppressed for ~140 s following coagulation. After 140 s, the SRS signal once again surpasses threshold. The spontaneous Raman signature is dominated by Raman scattering from the aqueous component. Unequal shifts of the TE and TM modes are clearly observed suggesting the existence of a decane layer on the surface of the aqueous droplet which varies with time, although the distortion of the WGMs observed in the spectra presented in Figure 6 is not apparent within the signal-to-noise of our measurements. The $TE_{46}$ mode is observed to shift to the red by 0.15 nm during the 60 s shown while the $TM_{45}$ mode shifts to the blue by 0.25 nm. The time variation in the mode offset of the TM mode from the two neighboring TE modes is shown in Figure 8b along with the time dependence of the thickness of the decane layer which can be directly correlated to film thickness from Mie scattering calculations for a core−shell droplet. Once the signature of the shell appears in the CERS fingerprint, the residual volume of decane would correspond to an organic shell of thickness 55 nm upon a spherical droplet 3.7 $\mu$m in radius. At long time, the shell does not evaporate further, suggesting that the gas and condensed phases are at equilibrium.

Although the uniformity of the coating and the sphericity of the droplet examined in Figure 6 have been questioned, the more symmetric nature of the resonant modes observed in this second example suggests that the droplet retains spherical symmetry and that the coating is approximately uniform. Given the surface tensions and interfacial tensions quoted in Section III, the spreading coefficient of decane on an aqueous sodium chloride surface is predicted to be ca. −1.7 mN/m at a salt concentration of ∼0.34 M. It is not possible to estimate the concentration of the inorganic salt in the aqueous phase in this droplet at long time as we cannot estimate accurately the initial volume of the aqueous component. However, it is not unreasonable to assume that after the time frame considered here the salt concentration in the aqueous phase is high enough to allow uniform spreading to occur. Accurate measurements of relative humidity would be required to test this explanation. Alternatively, it may be possible that all of the azimuthally degenerate modes traverse equivalent paths, sampling equal proportions of a bare aqueous surface and a surface coated in the organic component through the existence of a surface lens. In this case, they would sample the same mode volume and would appear at the same wavelength.

We finally return to consider the example presented in Figure 6. For second-order modes, the most intense internal field is located further from the droplet surface than the first-order mode.[43] Thus, significant deviations in the second-order mode offset for the layered droplet compared to the homogeneous droplet can be observed for layer thicknesses of up to 1.0 $\mu$m. Indeed, assuming the film is uniform and the droplet spherical, the core size is estimated to be 4.3 $\mu$m and the shell thickness 1.0 $\mu$m in this example. With such a "macroscopic" film situated on the surface of an aqueous droplet of similar dimensions, it is not surprising that the film is nonuniform and that the droplet does not retain spherical symmetry. Further experiments and a detailed theoretical treatment for simulating such nonuniform films will be required to explore such thick organic layers.

## V. Conclusions

We have demonstrated that optical tweezing coupled with Raman spectroscopy can be used to interrogate the mixing state and phase behavior of biphase organic/inorganic/aqueous aerosol droplets. The equilibrium configurations of decane/aqueous sodium chloride droplets depend on the initial sizes of the decane and the aqueous droplets prior to coagulation. The observed configurations of these multiphase droplets is shown to be consistent with a simple model on the basis of the surface and interfacial tensions of aqueous sodium chloride and decane. While a complete engulfing configuration is observed for small aqueous droplets within a large decane host droplet, complete engulfing of decane within an aqueous host droplet is not observed. The equilibrium geometry of the biphase droplet is observed to change with time as the two phases change in relative volume because of evaporation of the volatile constituent into the gas-phase.

Following evaporation of the decane component, the reappearance of SRS can be indicative of the formation of a core−shell structure in which the residual decane can be considered to spread on the surface of the concentrated salt solution droplet or forms a surface lens such that the WGMs remain degenerate. The mode offset arising from WGMs of different polarization provides an invaluable signature of the formation of such a structure. By comparing the WGM wavelengths apparent in the CERS fingerprint, the thickness of an organic shell on the surface of an aqueous droplet can be probed with 1 s time-resolution and with nanometer accuracy. Further, considerable distortion from sphericity is observed for thick organic layers, and it is suggested that the film is far from uniform. A fuller interpretation of this awaits a detailed theoretical analysis supported by further experimental observations.

Future work will seek to apply the optical tweezing technique described here in the characterization of the phase segregation and thermodynamic behavior of a broad range of organic/inorganic/aqueous aerosol droplets. Further, the ability to probe organic film thicknesses will be applied in systematic studies of the kinetics of mass transfer of the aqueous component through organic films of well-characterized thickness.[44]

**Acknowledgment.** We acknowledge the EPSRC for financial support and for supporting L.M. We also acknowledge the CCLRC for the award of facility time at the Lasers for Science Facility (CM1C1/05) and Dr. Andy Ward for his assistance at the early stages of this work. The Royal Thai government is acknowledged for studentship support for J.B.

## References and Notes

(1) Dick, W. D.; Saxena, P.; McMurry, P. H. *J. Geophys. Res.* **2000**, *105*, 1471.
(2) Zappoli, S.; Andracchio, A.; Fuzzi, S.; Facchini, M. C.; Gelencsér, A.; Kiss, G.; Krivácsy, Z.; Molnár, Á.; Mészáros, E.; Hansson, H.-C.; et al. *Atmos. Environ.* **1999**, *33*, 2733.
(3) Huebert, B.; Bertram, T.; Kline, J.; Howell, S.; Eatough, D.; Blomquist, B. *J. Geophys. Res.* **2004**, *109*, D19S11.
(4) Rogge, W. F. *Atmos. Environ.* **1993**, *27*, 1309.
(5) Hamilton, J. F.; Lewis, A. C.; Reynolds, J. C.; Carpenter, L. J.; Lubben, A. *Atmos. Chem. Phys.* **2006**, *6*, 4973.
(6) Kanakidou, M.; Seinfeld, J. H.; Pandis, S. N.; Barnes, I.; Dentener, F. J.; Facchini, M. C.; Van Dingenen, R.; Ervens, B.; Nenes, A.; Nielsen, C. J.; et al. *Atmos. Chem. Phys.* **2005**, *5*, 1053.
(7) Kalberer, M.; Paulsen, D.; Sax, M.; Steinbacher, M.; Dommen, J.; Prevot, A. S. H.; Risseha, R.; Weingartner, E.; Frankevich, V.; Zenobi, R.; Baltensperger, U. *Science* **2004**, *303*, 1659.
(8) Marcolli, C.; Luo, B. P.; Peter, Th. *J. Phys. Chem. A* **2004**, *108*, 2216.
(9) Marcolli, C.; Luo, B. P.; Peter, Th.; Wienhold, F. G. *Atmos. Chem. Phys.* **2004**, *4*, 2593.
(10) Pankow, J. F. *Atmos. Environ.* **2003**, *37*, 3323.
(11) Clegg, S. L.; Seinfeld, J. H.; Brimblecombe, P. *J. Aero. Sci.* **2001**, *32*, 713.
(12) McFiggans, G.; Artaxo, P.; Baltensperger, U.; Coe, H.; Facchini, C.; Feingold, G.; Fuzzi, S.; Gysel, M.; Laaksonen, A.; Lohmann, U.; et al. *Atmos. Chem. Phys. Discuss.* **2006**, *6*, 2593.
(13) Zhang, Q.; Worsnop, D. R.; Canagaratna, M. R.; Jimenez, J. L. *Atmos. Chem. Phys.* **2005**, *5*, 3289.
(14) Donaldson, D. J.; Vaida, V. *Chem. Rev.* **2006**, *106*, 1445.
(15) Russell, L. M.; Maria, S. F.; Myneni, S. C. B. *Geophys. Res. Lett.* **2002**, *29*, GL014874.
(16) Novakov, T.; Corrigan, C.; Penner, J.; Chuang, C.; Rosario, O.; Bracero, O. M. *J. Geophys. Res.* **1997**, *102*, 21307.
(17) Tervahattu, H.; Hartonen, K.; Kerminen, V. M.; Kupiainen, K.; Aarnio, P.; Koskentalo, T.; Tuck, A. F.; Vaida, V. J. *J. Geophys Res.* **2002**, *107*, D74053.
(18) Cai, X.; Griffin, R. J. *J. Geophys. Res.* **2003**, *108*, 4440.
(19) Hopkins, R. J.; Mitchem, L.; Ward, A. D.; Reid, J. P. *Phys. Chem. Chem. Phys.* **2004**, *6*, 4924.
(20) Reid, J. P.; Meresman, H.; Mitchem, L.; Symes, R. *Int. Rev. Phys. Chem.* **2006**, *26*, 139.
(21) Mitchem, L.; Buajarern, J.; Ward, A. D.; Reid, J. P. *J. Phys. Chem. B* **2006**, *110*, 13700.
(22) Mitchem, L.; Buajarern, J.; Hopkins, R. J.; Ward, A. D.; Gilham, R. J. J.; Johnson, R. L.; Reid, J. P. *J. Phys. Chem. A* **2006**, *110*, 8116.
(23) Torza, S.; Mason, S. G. *J. Coll. Inter. Sci.* **1970**, *33*, 67.
(24) Horibe, A.; Fukusako, S.; Yamada, M. *Int. J. Thermophys.* **1996**, *17*, 483.
(25) *CRC Handbook of Chemistry and Physics: A Ready-Reference Book of Chemical and Physical Data*; Lide, D. R., Ed.; CRC: Boca Raton, FL, 2003.
(26) Shaw, D. J. *Introduction to Colloid & Surface Chemistry*; Butterworth-Heinemann: Oxford, 1992.
(27) Knox, K. J.; Reid, J. P.; Handford, K. L.; Hudson, A. J.; Mitchem, L. *J. Opt. A: Pure Appl. Opt.* 2007, in press.
(28) Mitchem, L.; Hopkins, R. J.; Buajarern, J.; Ward, A. D.; Reid, J. P. *Chem. Phys. Lett.* **2006**, *432*, 362.
(29) Reid, J. P.; Mitchem, L. *Annu. Rev. Phys. Chem.* **2006**, *57*, 245.

(30) Ray, A. K.; Nandakumar, R. *Appl. Opt.* **1995**, *34*, 7759.
(31) Chen, G.; Chang, R. K.; Hill, S. C.; Barber, P. W. *Opt. Lett.* **1991**, *16*, 1269.
(32) Chylek, P.; Videen, G.; Ngo, D.; Pinnick, R. G.; Klett, J. *J. Geophys. Res.* **1995**, *100*, 16325.
(33) Chylek, P.; Lesins, G.; Videen, G.; Wong, J.; Pinnick, R. G.; Ngo, D.; Klett, J. *J. Geophys. Res.* **1996**, *101*, 23365.
(34) Eversole, J. D.; Lin, H.-B.; Campillo, A. J. *J. Opt. Soc. Am. B* **1995**, *12*, 287.
(35) Ma, X.; Lu, J. Q.; Brock, R. S.; Jacobs, K. M.; Yang, P.; Hu, X.-H. *Phys. Med. Biol.* **2003**, *48*, 4165.
(36) Swindal, J. C.; Leach, D. H.; Chang, R. K.; Young, K. *Opt. Lett.* **1993**, *18*, 191.
(37) Han, Y.; Mees, L.; Gouesbet, G.; Wu, Z.; Grehan, G. *J. Opt. Soc. Am. B* **2006**, *23*, 1390.
(38) Lu, J. R.; Thomas, R. K.; Binks, B. P.; Fletcher, P. D. I.; Penfold, J. *J. Phys. Chem.* **1995**, *99*, 4113.
(39) Aden, A. L.; Kerker, M. *J. Appl. Phys.* **1951**, *22*, 1242.
(40) Ray, A. K.; Souyri, A.; Davis, E. J.; Allen, T. M. *Appl. Opt.* **1991**, *30*, 3974.
(41) Wiscombe, W. J. FORTRAN Subroutine for the Calculation of Light Scattering by Coated Spheres; ~ftp://climate.gsfc.nasa.gov/pub/wiscombe/Single-Scatt/Coated-Sphere/ (accessed 1993).
(42) Millard, R. C.; Seaver, G. *Deep-Sea Res.* **1990**, *37*, 1909.
(43) Symes, R.; Sayer, R. M.; Reid, J. P. *Phys. Chem. Chem. Phys.* **2004**, *6*, 474.
(44) Chan, M. N.; Chan, C. K. *Atmos. Environ.* **2007**, *41*, 4423.